2018 IEEE/RSJ International Conference on Intelligent Robots and Systems (IROS)
Madrid, Spain, October 1-5, 2018

# Material Recognition Using a Capacitive Proximity Sensor with Flexible Spatial Resolution

Hosam Alagi[1], Alexander Heilig[1], Stefan Escaida Navarro[2]
Torsten Kroeger[1] and Björn Hein[1]

***Abstract*— In this paper we present an approach for material recognition using capacitive tactile and proximity sensors. By variating the spatial resolution and the exciter frequency during the measurement in mutual capacitive mode, information about the dielectrical properties of different objects was captured and provided as data frames. For material recognition an artificial neural network was set up and fed with various data sets of different electrode combinations and exciter frequencies. The influence of the electrode combinations and shapes on the recognition accuracy was investigated. It is shown that seven objects of conductive and non-conductive dielectric materials have been ranged with an overall accuracy of about $71\% - 94\%$.**

## I. INTRODUCTION

Sensor skins for robots are nowadays considered to be a standard component for service robotics and also industrial robots in the context of HRI. Traditionally, the skin is used to detect a contact interaction. More recently, there has been a trend towards including the ability to detect objects/events in the near proximity of the robot, that is, before a touch event happens. To this end, several measurement principles have been proposed based on different physical effects, mainly acoustic, optical and capacitive; examples are [1], [2], [3] respectively. When making a proximity measurement the signal carries information about some physical properties of the object due to the specific measurement principle, like its optical reflectance or acoustic absorption properties, etc. Therefore, it is natural to ask if one can extract additional properties of the object from the signal used for proximity measurements. Our line of work has been dedicated to designing hardware and applications for capacitive tactile and proximity sensing. Capacitive sensing is affected by the electrical properties of the object (conductivity, permittivity when non-conducting), its size and shape and of course its distance to the sensor. In this work we propose a sensor hardware and machine learning approach for object material recognition based on the permittivity of the objects. With this, it is possible for the robot to explore its workspace beyond visual and haptic features. One example of an interesting application in service robotics would be the manipulation of containers. Robots can be made more intelligent by knowing if a container (cereal box or cup, etc.) is filled with liquid or other materials, even though it might be nontransparent.

Fig. 1. With the sensors mounted on an end-effector the robot can perceive objects in its workspace and classify them according to their permittivity or conductivity.

The research presented here is a continuation of our previous work [4], where we introduced a capacitive tactile proximity sensor for applications in robotics and consumer electronics. Besides minimizing the main PCB and adding an interface PCB for connecting different electrodes via Coaxial cable, we increased the possible connected electrodes from 4 to 8. We also established a further connection to synchronize multi-sensor modules. Fig. 1 shows three of our sensor modules as part of an end-effector that is approaching a wooden ball. One of the main characteristics of the sensor is its ability to reconfigure its spatial resolution on-line by merging the electrodes using an analog switch. This increases the measurement area of the resulting electrode and thus the sensitivity of the measurement. Depending on how the reconfiguration is done, different electrode geometries can be implemented.

In this paper we present the upgrades made to this sensor

*This research was funded by the German Research Foundation (DFG) under the grants HE 7000/1-1 and WO 720/43-1.

[1]Authors are with Institute for Anthropomatics and Robotics - Intelligent Process Control and Robotics Lab (IAR-IPR), Karlsruhe Institute of Technology {hosam.alagi, bjoern.hein, torsten.koeger}@kit.edu, alexander.heilig2@student.kit.edu

[2]Stefan Escaida Navarro is with the team Defrost at Inria Lille-Nord Europe stefan.escaida-navarro@inria.fr

and how it can be used for a material recognition task. The rest of the paper is structured as follows: After this introduction the state of the art is presented in Section II. In Section III we present our sensing system used to collect the data about the different objects. In Section IV we discuss the experiments in material recognition and their results. Finally, in Section V, we provide a summary and give conclusions for this paper.

## II. Related Work

Like stated in the introduction, capacitive proximity measurements have the potential to be used to identify material. More specifically, the materials are represented by the relative permittivity $\varepsilon_r$. One way to identify different dielectrical materials is to measure their permittivity. When the task is to distinguish between different materials in a set, it is already sufficient to compare their relative permittivity. In general this can be done by gathering sample data and then applying classification methods. Kirchner et al. proposed data generated by using three discrete frequencies [5] to classify four classes of objects (concrete, human, metal and wood). The use of different frequencies is decisive for their results. By driving the sensor towards the object, a distance dependent curve was recorded which was then used for the material ranging. In our work we also use different frequencies, but we propose an approach which only depends on the sensor values. In other words, a single frame of sensor measurements is used to predict the material.

Using frequency sweep instead of discrete multi-frequencies can provide even more precise material ranging. König et al. [6] presented a device based on the impedance analyzer AD5933 combined with a temperature and a color sensor. By analyzing the data of the three sensors, "Lab-on-Spoon" is even able to distinguish between different sorts of wine or beer. Another interesting approach for an impedance analyzer using magnetic and electric component is shown by Yunus et al. and Wang et al. [7] and [8] respectively. Both works target the same application domain regarding water pollution detection. They try to distinguish and quantify the contamination caused by nitrate and phosphate for example and both use planar sensors driving frequencies between $20\,\mathrm{Hz}$ and $5\,\mathrm{MHz}$. In all three works, the material to be detected accounts for all the dielectric between the electrodes of the capacitor. The displacement field goes through the material only, i.e the determined capacitance results from this material. In our approach, the objects account for about 20% of the dielectric material between the electrodes of the capacitor; the rest is air. Still, by varying the electrode area, shape and exciter frequencies, information about the object material can be collected.

Wang et al. specifically investigated different electrode designs in [8]. Due to the fact that significant changes in the signal have been observed in permittivity at frequencies below $500\,\mathrm{kHz}$ and that the shape and the order of the electrodes are major for the measurement, we see the analogy to our sensor in the multi-frequency measurement and the dynamic electrode configuration. However, our approach is less complex using two discrete frequencies and the electrode reshaping was realized by the flexible spatial resolution of the sensor.

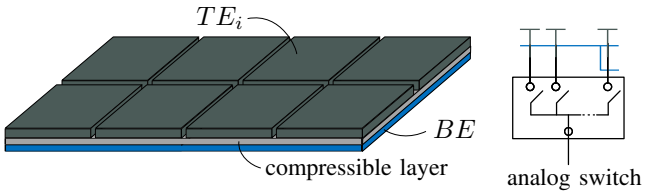


Fig. 2. The assembly of a sensing element for the sensing together with an analog switch for electrode selection and combination [4].

The influence of the electrode shapes on the distribution of the potential field and thus the displacement field lines plays a key role in analyzing dielectric material. The work of Yin addresses this issue in [9]. In order to derive design principles for so called "Capacitive Imaging - CI", different parameters, *shapes*, *number*, *separation* of electrodes and the *peak-to-peak voltage* of the exciter signal in a *frequency range* of $10\,\mathrm{kHz}-1\,\mathrm{MHz}$ have been variated. A further related term to our work is the "capacitive tomography". Such a system uses multiple capacitive sensors or multi-electrode system to scan a dielectric material. An overview regarding the hardware design is given in [10]. In [11] this has been done by variating the distribution of the electric-field intensity in an object through different electrode combinations in order to extract geometrical information about the test object. A simple capacitive proximity sensor with one exciter frequency and fixed electrodes would not provide enough information about detected objects. Therefore, A.Kimoto in [12] combined optical sensor with capacitive one. He was able to distinguish between Acrylic, PTFE, Class and Aluminum in different surface properties. In the context of robotics and especially in grasping applications collecting information about the object is essential. In such scenarios a gripper or manipulator equipped with suitable capacitive sensors can provide internal properties of the object's material. Respectively, the control system can then decide which object should be grasped [13]. In this case the capacitive sensor provides information which is complementary to those of vision or haptics. Beyond the material recognition, we aim in this work to improve the used capacitive *tactile* and *proximity* sensors by adding new features and still keeping the system as simple as possible for robotics.

The fact that we develop our own sensor system enables us to implement new features such as the flexible special resolution and using multi-frequencies for the exciter signal. Many manufactures offer own solutions e.g. MGC3x30 for 3D gesture recognition and motion tracking from Microchip Technology, Cypress Semiconductor CapSense® for Proximity Sensing or AD7150 a complete signal processing solution for capacitive proximity sensors from Analog Devices. Those products are limited when it comes to instigate new methods beyond the their defined applications.

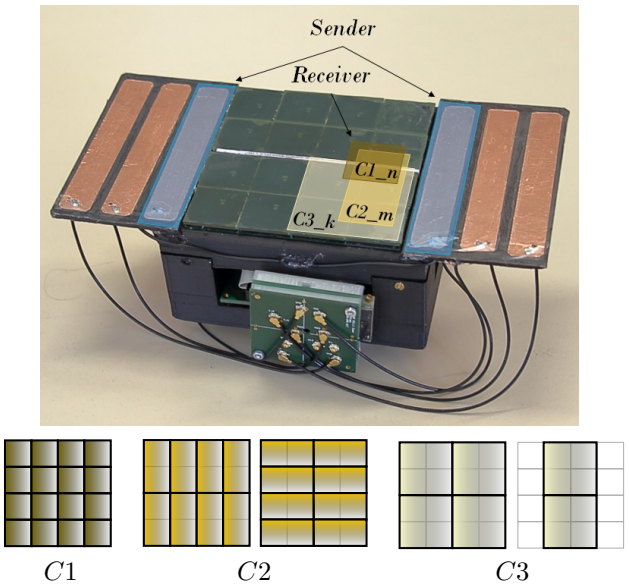


Fig. 3. The end-effector featuring three sensor modules: two 4×2 modules in the middle configured in receive mode and one module driving up to six electrodes in send mode. The PCB with the analog and digital electronics for the third module is visible in the front. The three modules are connected to the same I2C bus. It is also illustrated how the flexible spatial resolution is used to select single electrodes $C1_n$ with $n \in \{1, \ldots, 16\}$, configurations of two electrodes combined $C2_m$ with $m \in \{1, \ldots, 16\}$ and configurations of four electrodes combined $C3_k$ with $k \in \{1, \ldots, 6\}$.

## III. System Description

In this section we present the general sensor design and then the concrete hardware implementation. We give an overview of the use of the flexible spatial resolution. At the end we discuss the background of the frequency dependent permittivity.

### A. Sensor Design

In this sub-section, a brief outline of the general sensor design is given. The design, which was presented in [4], consists of a sensing element, depicted in Fig. 2, and the analog and digital electronics needed for driving the sensor shown in Fig. 3. The sensor can be used in *self-capacitive* (send) and *mutual-capacitive* (receive) mode. Both modes are alternatively called *single-ended* and *double-ended* in literature. In the self-capacitive mode the top electrodes ($TE_i$) are driven with an AC signal passing through the analog switch, which can select or join electrodes arbitrarily. The signal causes the periodic charging and discharging of the electrodes. The capacitive coupling of the configuration with the environment can be measured by finding the amplitude of the current flowing through the circuit. To guide the coupling towards the "outside" side of the sensor, the bottom electrode $BE$ is used to actively shield the $TE_i$ from any components below. An object will affect the coupling according to its material properties and its proximity to the sensor. In the mutual-capacitive receive mode the $TE_i$ are connected to ground through a measurement circuit. In the presence of a sender there will be an electric field configuration showing from the sender towards the receiver, inducing a current at the receiver side. An object near the electrodes will affect the field configuration. This effect is reflected in the current being measured and again depends on the object properties. This double-ended measurement is suited for detecting insulated objects with a high enough relative permittivity. With our sensor a tactile measurement is also possible due to the compressible, insulating layer between $TE_i$ and $BE$, but it is not used in this work. Finally, the frequency of the exciting signal can be adjusted, which is also an important aspect for material recognition, since the permittivity can be a frequency dependent value (see Sec. III-C).

### B. Sensor Hardware

The actual hardware sensors can be seen in Fig. 3. Two 4×2 modules combined make up the receiver array of the end-effector. A third module acts as a sender. Six of its electrodes are installed at both sides of the receiver array, although in this work only the ones closest to the receivers have been activated (represented by blue stripes). In this work, the flexible spatial resolution is used to take measurements with different electrode sizes and shapes, as seen Fig. 3. At each resolution the set of measurements can be thought of as a capacitive image. The collection of all measurements then is a multi-resolution capacitive image, which we call a *frame*. The hardware sequentially generates a frame within some fraction of a second by time-multiplexing through each configuration of electrodes. The end-effector is mounted on a 6-Axes-Robot and Robot Operating System *(ROS)* is used as a middleware. For generating and executing the trajectories *MoveIt* and *ROS Control* are used. By reshaping the electrodes we assume to get different configuration of the potential field and thus the penetration or polarization of the dielectric objects by the electrical field. Figure 3 shows the configurations used for the measurements, where three basic electrode combinations are highlighted. An electro static simulation shows in Fig. 4 how the potential field is affected by different electrode combinations for the same object. The simulation was run for wooden ball with a relative permittivity of 9.4.

### C. Frequency Dependent Permittivity

In this sub-section we discuss the dependency of the permittivity on the frequency of the exciting signal. Sender and receiver represent the two electrode plates of a capacitor. Because the wavelength of the signal is large compared to the electrodes, the quasi-static assumption can be used. The amount of the charges in the static case can be calculated by the first Maxwell equation:

$$Q = \oint D \, dA = \oint \varepsilon_0 \varepsilon_r E \, dA \tag{1}$$

where D is the displacement field vector, E the electrical field vector, $\varepsilon$ the permittivity and A is the path enclosing the vector field. $\varepsilon E_0$ and $\varepsilon E_r$ are the absolute and the relative permittivity. The latter depends on the medium between the electrodes and describes its dielectric properties. $\varepsilon E_0$

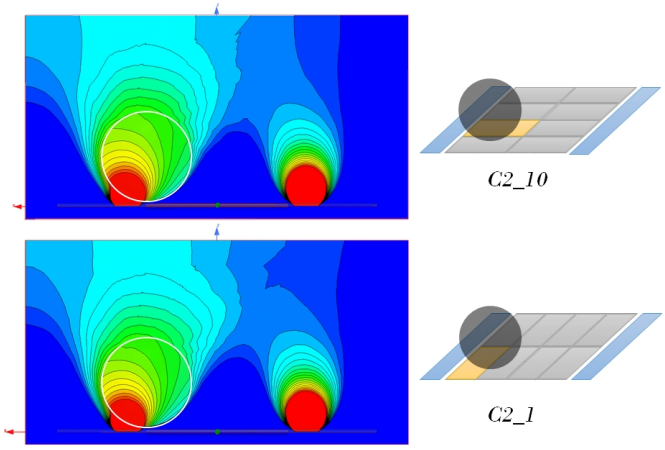


Fig. 4. Electro-statical simulation of the potential field of three electrode combinations $(C1_1, C2_1, C3_k)$ for wooden object, $\varepsilon_r = 2,7$. Slight difference in the field distribution between the electrode combinations can be seen.

is constant; $8,854 \cdot 10^{-12} \frac{F}{m}$. By including the frequency dependency, the equation becomes:

$$Q(\omega) = \oint \varepsilon_0 \varepsilon_r(\omega) E \, dA \tag{2}$$

where $\omega$ is the angular frequency of the exciter signal. Making the following assumptions:

- The electrode is shielded at the bottom side (through $BE$),
- stray fields can be neglected and
- the source voltage is constant (which in our case means it has a constant amplitude)

then, the charge is affected by $\varepsilon_r(\omega)$. The charge $Q$ can indirectly be determined by measuring the current at the sender or receiver. In the case of very good conductive material and at such frequencies used in this work, one may assume the the $\varepsilon_r \approx 1$ and frequency independent [14, p. 500]. The conductivity is as high as the one of the electrodes, which makes the Object acting as an coupling electrode between the sensor and the ground.

## IV. Evaluation and Results

In this section we discuss the experimental setup, the framework and setup for learning with artificial neural networks (ANNs) and the results obtained using different combinations of electrode configurations and signal frequencies.

### A. Experimental Setup

To evaluate the system, the objects listed in Table I were used.[1] It is worth mentioning that the relative permittivity of wood strongly depends on its water content. In this work we consider the water content in percentage at about 15-20%. In general, the values in Table I. All experiments were done in the laboratory by constant ambient temperature and humidity. The distance between the electrode array and the top of the objects is kept to $2\,\mathrm{mm}$ during the measurements. The end effector is moved in a meander path over the objects enclosing the borders of the receiver array. Fig. 6 shows the initial position of the end-effector and the followed path. This path is iterated ten times while the data is collected. In the training phase 74033 samples of all material were split in proportion 8/2 for training/validation. Additional 18512 samples were recorded for test. Every sample is a frame that contains the sensor values for the various electrode combinations and frequencies. Its size could variate depending on the selected combinations.

[1]The table is an excerpt of the values found in http://www.kayelaby.npl.co.uk/general_physics/2_6/2_6_5.html

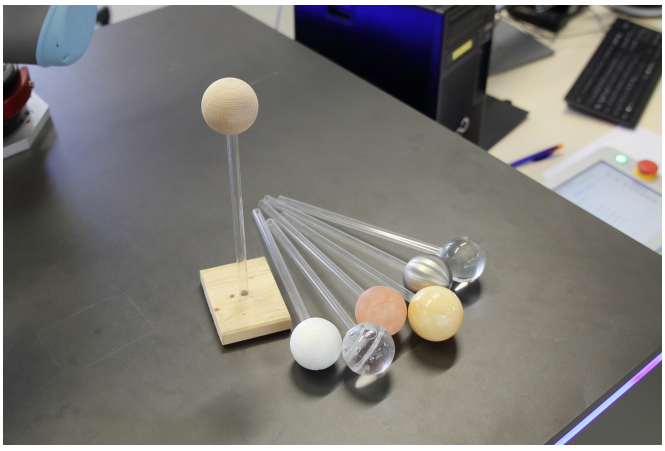

Fig. 5. Balls with diameter of $5cm$; Test objects of different Materials, one ball each

| Material | Relative Permittivity $\varepsilon_r$ |
|---|---|
| Styrofoam[15] | 1.03 |
| Glass (quartz) | 3.8 |
| Salt (NaCl) | 6.1/5.9 |
| Marble | 8.0 |
| Wood (Beech 16% water) | 9.4/8.5 |
| Tap water | 80.1 |

TABLE I
RELATIVE PERMITTIVITY OF THE USED TEST MATERIALS

### B. Artificial Neural Network

The material recognition neural network has been implemented in *Tensorflow 1.3.0*. The recorded data was trained using a feed-forward neural network (ANN). For the ANN, the number of the input neurons was defined as the size of the

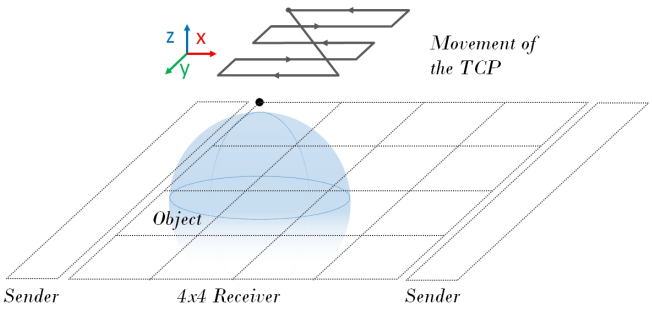


Fig. 6. Initial position of the end effector and its path

| | |
|---|---|
| Hidden layers | 400, 400 |
| Batch size | 300 |
| Learning rate | 0,001 |
| L2 beta | 0,1 |
| Dropout | 0,1 |

TABLE II

HYPERPARAMETERS OF THE ANN

data frames, hence by the selected electrode combinations and frequencies for each data set. The input was then forwarded through a series of *ReLU-layers*, where a dropout rate of 10% had been set. Lastly, the data was fed to a *softmax* output layer, whose size equaled the amount of materials trained for. In addition to introducing dropout to all hidden layers, the weights were also modified through L2 regularization to further decrease overfitting. Updates to weights were done in mini-batches of 300 and optimized by the Adam optimizer [16]. To further prevent overfitting, every five epochs, the validation set's accuracy was calculated and training was prematurely ended when this accuracy exceeded a threshold of 0.98. Furthermore, a patience period of ten epochs to stop training was set, which counted up if the validation loss did not decrease compared to the last best loss. The best results were achieved by setting the hidden layer size to two layers with 400 units each. The initial learning rate was set to 0.001. The Hyperparameters are listed in Table II. Those were determined in a previous experimental run and showed best results for all data sets. The hyper-parameter do not variate between the data sets.

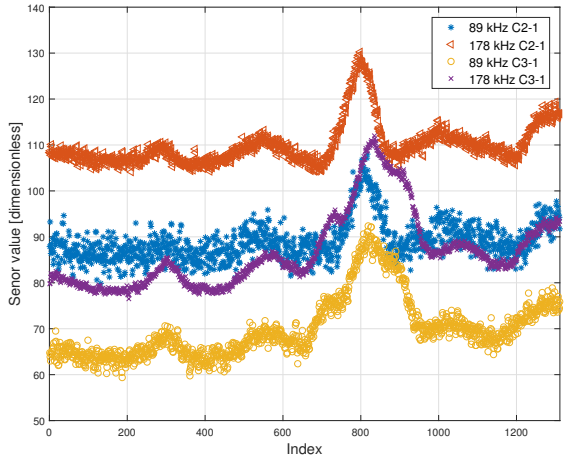


Fig. 7. Data of the electrode combinations $C2_1$, $C3_1$ and both frequencies

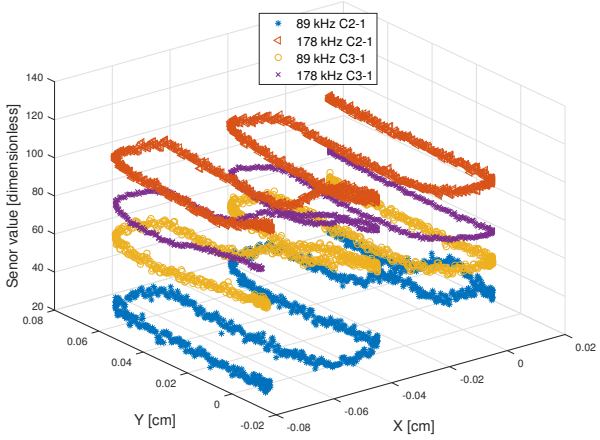


Fig. 8. Data of the electrode combinations $C2_1$, $C3_1$ and both frequencies plotted over the movement of the end effector

## C. Results

The measurement is performed for all seven objects[2] as described in Sec. IV-A. For each object about 13100 data frames are collected. Due to the air-like relative permittivity of "styrofoam" this object acted as air. A closer look at the data of styrofoam shows that neither of the combinations was affected by the object. As an example, Fig. 7 and 8 present a data set of the metal object for the combinations $C2_1$, $C3_1$ and both frequencies respectively in 2D and 3D plot. The latter one is plotted over the path of the end effector in xy-plane.

| | |
|---|---|
| Set | 1 |
| variation | $C1_n$, $C2_m$, $C3_k$ 89 kHz,178 kHz |
| Input | 76 |
| Epochs trained | 30 |
| Test accuracy | 93.2% |

| $me$ | $sa$ | $ma$ | $wo$ | $gl$ | $wa$ | $sf$ |
|---|---|---|---|---|---|---|
| 2685 | 0 | 0 | 0 | 0 | 0 | 0 |
| 0 | 2102 | 557 | 0 | 1 | 0 | 0 |
| 0 | 553 | 2126 | 0 | 0 | 0 | 0 |
| 0 | 0 | 0 | 2465 | 144 | 0 | 23 |
| 0 | 0 | 0 | 0 | 2640 | 0 | 0 |
| 0 | 0 | 0 | 0 | 0 | 2607 | 0 |
| 0 | 0 | 0 | 0 | 0 | 0 | 2630 |

| | |
|---|---|
| Accuracy | 93.2% |
| Precision | [100 79.7 79.2 100 94.8 100 99.1] |
| Recall | [100 79.8 79.2 100 94.8 100 99.1] |

[2]me: metal, sa: salt, ma: marble, wo: wood, gl: glass, wa: water, sf: styrofoam

| | |
|---|---|
| Set | 2 |
| Variation | $C1_n$ |
| | 89 kHz,178 kHz |
| Input | 32 |
| Epochs trained | 100 |
| Test accuracy | 81.9% |

| $me$ | $sa$ | $ma$ | $wo$ | $gl$ | $wa$ | $sf$ |
|---|---|---|---|---|---|---|
| 2675 | 0 | 0 | 0 | 8 | 2 | 0 |
| 0 | 2249 | 410 | 0 | 1 | 0 | 0 |
| 0 | 714 | 1945 | 0 | 0 | 0 | 0 |
| 0 | 0 | 0 | 1697 | 0 | 536 | 399 |
| 0 | 0 | 0 | 1254 | 1376 | 3 | 7 |
| 12 | 0 | 0 | 0 | 0 | 2595 | 0 |
| 0 | 0 | 0 | 0 | 0 | 0 | 2630 |

| | |
|---|---|
| Accuracy | 81.9% |
| Precision | [99.6 84.6 73.1 64.5 52.1 99.5 100] |
| Recall | [99.5 75.9 82.6 57.5 99.4 82.7 86.6] |

| | |
|---|---|
| Set | 3 |
| Variation | $C2_m$ |
| | 89 kHz,178 kHz |
| Input | 32 |
| Epochs trained | 25 |
| Test accuracy | 94.2% |

| $me$ | $sa$ | $ma$ | $wo$ | $gl$ | $wa$ | $sf$ |
|---|---|---|---|---|---|---|
| 2665 | 20 | 0 | 0 | 8 | 2 | 0 |
| 2 | 1835 | 822 | 0 | 1 | 0 | 0 |
| 0 | 223 | 2436 | 0 | 0 | 0 | 0 |
| 0 | 0 | 0 | 2632 | 0 | 0 | 0 |
| 0 | 0 | 0 | 0 | 2640 | 0 | 0 |
| 0 | 0 | 0 | 0 | 0 | 2607 | 0 |
| 0 | 0 | 0 | 0 | 3 | 0 | 2627 |

| | |
|---|---|
| Accuracy | 94.2% |
| Precision | [99.3 69.0 91.6 100 100 100 100] |
| Recall | [99.9 88.3 74.8 100 100 100 100] |

| | |
|---|---|
| Set | 4 |
| Variation | $C3_k$ |
| | 89 kHz,178 kHz |
| Input | 12 |
| Epochs trained | 100 |
| Test accuracy | 71.2% |

| $me$ | $sa$ | $ma$ | $wo$ | $gl$ | $wa$ | $sf$ |
|---|---|---|---|---|---|---|
| 2401 | 0 | 0 | 1 | 194 | 89 | 0 |
| 0 | 2195 | 464 | 0 | 1 | 0 | 0 |
| 0 | 1200 | 1259 | 0 | 0 | 0 | 0 |
| 33 | 0 | 0 | 416 | 16 | 2150 | 7 |
| 293 | 0 | 0 | 754 | 1584 | 9 | 0 |
| 0 | 0 | 0 | 0 | 0 | 2607 | 0 |
| 0 | 0 | 0 | 0 | 3 | 0 | 2627 |

| | |
|---|---|
| Accuracy | 71.2% |
| Precision | [89.4 82.5 51.1 15.8 60.0 100 99.9] |
| Recall | [88.0 62.8 74.5 35.5 87.7 53.7 99.7] |

The network was fed with different combinations of the measurement regarding the electrode combinations and the exciter frequencies. We assumed that the maximum information content is given by an input data set including all combinations. Therefore, the trained network with $C1_n$, $C2_m$, $C3_k$ and both frequencies is set as a reference network regarding the listed parameters in $Set1$.

To identify the contribution of each electrode combination to the accuracy achieved by $Set1$, the three following sets have been tested. The electrode combinations $C1_n$, $C2_m$ and $C3_k$ each for two frequencies were tested respectively in $Set2$, $Set3$ and $Set4$. The sets show disparate results where $C1_n$ and $C3_k$ reach a modest accuracy of $82\%$ and $71\%$ by training over 100 epochs, the maximum amount specified. $Set3$ shows the best accuracy of $94\%$ with 25 epochs trained. We believe that the $C1_n$ and $C3_k$ do not provide enough information. While $C1_n$ has the highest spatial resolution, its electrodes are relatively small and less sensitive, lower Signal-to-Noise ratio (SNR). On the other hand, $C3_k$ has the highest sensitivity, but also the lowest spatial resolution. $C2_m$ provides the spatial resolution of $C1_n$ and increased sensitivity.

Apparently water was very well identified by the network, which is plausible due to their high relative permittivity. Styrofoam, which was considered as air, was easily identified, too. Marble and salt had a lower accuracy by being wrongly predicted as the other one, which is plausible due to their similar relative permittivity. Wood was misidentified in some cases with other materials except marble and salt. The scattered values of ungrounded metal, which is supposed to have its own characteristic, were unexpected. Regarding the results of the last three sets the $C2_k$ combination showed the best results, since the objects were perceived with higher sensitivity than $C1_k$ and more detail than $C3_k$. To get homogeneous frames regarding the spatial resolution we would investigate in future works in sensor overlapping electrode combinations, which is for now limited by the sensor hardware.

## V. Conclusion

In this work we presented an approach for material recognition using multi-frequency capacitive tactile and proximity sensors with flexible spacial resolution and an artificial neural network for the classification. The essence of the work was to perform the measurement with various combination of the sensor features which can provide sufficient information to recognize material without further information. For the evaluation, data has been collected by measuring seven object of different materials with variation of electrode combinations and two driving frequencies. The data sets were split up in training and test data and fed to a feed-forward network with two hidden layers of 400 units each. The best recognition result with an accuracy of $94\%$ was reached through the $C2_m$ electrode combination and both frequencies. Across the different models the worst recognition precision of $16\%$ was obtained from wood. Furthermore, confusion was recorded between marble and salt. However, the experiment shows that the combination of various electrode shapes and driving frequencies is promising for material recognition. In the

robotics such a system provides an important ingredient for an intelligent robot. Since all experiments were done in the laboratory by constant ambient temperature and humidity. Further investigation in operating conditions should also be done.

## REFERENCES


[1] L.-T. Jiang and J. R. Smith, "Seashell effect pretouch sensing for robotic grasping," in *2012 IEEE International Conference on Robotics and Automation*, May 2012, pp. 2851–2858.

[2] K. Koyama, Y. Suzuki, A. Ming, and M. Shimojo, "Integrated control of a multi-fingered hand and arm using proximity sensors on the fingertips," in *2016 IEEE International Conference on Robotics and Automation (ICRA)*, 2016, pp. 4282–4288.

[3] T. Schlegl, T. Krger, A. Gaschler, O. Khatib, and H. Zangl, "Virtual whiskers #x2014; Highly responsive robot collision avoidance," in *2013 IEEE/RSJ International Conference on Intelligent Robots and Systems*, Nov. 2013, pp. 5373–5379.

[4] H. Alagi, S. E. Navarro, M. Mende, and B. Hein, "A versatile and modular capacitive tactile proximity sensor," in *2016 IEEE Haptics Symposium (HAPTICS)*, Apr. 2016, pp. 290–296.

[5] N. Kirchner, D. Hordern, D. Liu, and G. Dissanayake, "Capacitive sensor for object ranging and material type identification," *Sensors and Actuators A: Physical*, vol. 148, no. 1, pp. 96–104, Nov. 2008. [Online]. Available: http://www.sciencedirect.com/science/article/pii/S0924424708004184

[6] A. Knig and K. Thongpull, "Lab-on-Spoon a 3-D integrated hand-held multi-sensor system for low-cost food quality, safety, and processing monitoring in assisted-living systems," *Journal of Sensors and Sensor Systems*, vol. 4, no. 1, pp. 63–75, Feb. 2015. [Online]. Available: https://www.j-sens-sens-syst.net/4/63/2015/

[7] M. A. M. Yunus, S. C. Mukhopadhyay, and S. Ibrahim, "Planar Electromagnetic Sensor Based Estimation of Nitrate Contamination in Water Sources Using Independent Component Analysis," *IEEE Sensors Journal*, vol. 12, no. 6, pp. 2024–2034, June 2012.

[8] X. Wang, Y. Wang, H. Leung, S. C. Mukhopadhyay, M. Tian, and J. Zhou, "Mechanism and Experiment of Planar Electrode Sensors in Water Pollutant Measurement," *IEEE Transactions on Instrumentation and Measurement*, vol. 64, no. 2, pp. 516–523, Feb. 2015.

[9] X. Yin, D. A. Hutchins, G. Chen, and W. Li, "Preliminary studies on the design principles of capacitive imaging probes for non-destructive evaluation," *International Journal of Applied Electromagnetics and Mechanics*, vol. 42, no. 3, pp. 447–470, Jan. 2013. [Online]. Available: https://content.iospress.com/articles/international-journal-of-applied-electromagnetics-and-mechanics/jae01676

[10] W. Yang, "Design of electrical capacitance tomography sensors," *Measurement Science and Technology*, vol. 21, no. 4, p. 042001, 2010. [Online]. Available: http://stacks.iop.org/0957-0233/21/i=4/a=042001

[11] I. Matiss, "Multi-element capacitive sensor for non-destructive measurement of the dielectric permittivity and thickness of dielectric plates and shells," *NDT & E International*, vol. 66, pp. 99–105, Sept. 2014. [Online]. Available: http://www.sciencedirect.com/science/article/pii/ S0963869514000735

[12] A. Kimoto, S. Fujisaki, and K. Shida, "A proposal of new contactless layered sensor for material identification," *Sensors and Actuators A: Physical*, vol. 155, no. 1, pp. 33–38, Oct. 2009. [Online]. Available: http://www.sciencedirect.com/science/article/pii/ S0924424708004779

[13] S. Mhlbacher-Karrer, A. Gaschler, and H. Zangl, "Responsive fingers #x2014; capacitive sensing during object manipulation," in *2015 IEEE/RSJ International Conference on Intelligent Robots and Systems (IROS)*, Sept. 2015, pp. 4394–4401.

[14] P. Lorrain, D. R. Corson, and F. Lorrain, *Electromagnetic Fields and Waves*, third edition ed. W.H.Freeman & Co, 1988.

[15] H. J. Visser, "Appendix D: Physical Constants and Material Parameters," in *Antenna Theory and Applications*. John Wiley & Sons, Ltd, 2012, pp. 243–244. [Online]. Available: http://onlinelibrary.wiley.com/doi/10.1002/9781119944751.app4 /summary

[16] D. P. Kingma and J. Ba, "Adam: A method for stochastic optimization," *CoRR*, vol. abs/1412.6980, 2014. [Online]. Available: http://arxiv.org/abs/1412.6980